RSC Advances

PAPER

View Article Online
View Journal | View Issue

Cite this: *RSC Adv.*, 2022, **12**, 32129

Slower diffusion and anomalous association of R453W lamin A protein alter nuclear architecture in AD-EDMD†

Chandrayee Mukherjee, ‡[a] Duhita Sengupta, ‡[a] Lakshmi Maganti,‡[b] M. Mahendar,[a] Dhananjay Bhattacharyya [b] and Kaushik Sengupta *[a]

Lamins maintain the shape and rigidity of the nucleus in the form of a proteinaceous scaffold underneath the inner nuclear membrane (INM) and provide anchorage to chromatin and other nuclear proteins. Mutations in the human LMNA gene encoding lamin A/C cause about 16 different diseases with distinct phenotypes collectively termed as laminopathies which affect primarily the muscle tissues as well as adipose tissues, neuromuscular junctions and multiple other organs in progeroid syndromes. Lamins contain several domains of which Ig-fold is one of the well characterized and structured domains that harbours many mutations leading to deleterious interactions with other nuclear proteins. In this work, we have elucidated the effects of 3 such mutations namely R453W, W498C and W498R on the dynamics and flexibility of the Ig-fold domain and the consequent effect on the assembly into lamina by live cell imaging, fluorescence correlation spectroscopy (FCS) and molecular dynamics (MD) simulations. From our simulation studies, we concluded that R453W exhibits the highest fluctuation at the residues 475 and 525 in the Ig fold domain compared to the wild type and other mutants. This resulted in pronounced random self-association which could be corroborated by lower diffusivity values obtained from FCS. This is the first report where such an alteration in the full length has been documented by gross changes in diffusional properties as a sequel to a mutation in the Ig fold domain.

Received 6th September 2022
Accepted 28th October 2022

DOI: 10.1039/d2ra05620h

rsc.li/rsc-advances

Introduction

A and B-type lamins are intermediate filament proteins and form a fibrous network in the nucleoplasmic space beneath the INM of all terminally differentiated metazoan cells except plants.[1–4] The lamins constitute the scaffold for the nuclear envelope and facilitate tethering of chromatin and other nuclear proteins.[4] Structurally, lamins possess a characteristic tripartite structure unique to the intermediate protein family. The central coiled-coil forming the α-helical portion of lamins is flanked by a short unstructured 'head' domain at its N-terminal and by a longer C-terminal domain.[5–7] The C-terminal domain is grossly unstructured except for a small island of an ~113 residue long globular motif consisting of nine β strands thus conferring it a classical Immunoglobulin fold (Ig-fold) architecture.[8,9] The sandwich-like structure of two β sheets consisting of 5 and 4β strands respectively are connected by short loops.[10] The C-terminal domain harbours binding sites for chromatin[11] as well as other nuclear proteins like PCNA, LAP2α, emerin *etc.*[12,13] Furthermore, the Ig-fold domain maintains a unique status due to its interaction with PCNA,[14] Nup proteins and harbouring a site of interaction with SUMOylated substrates.[15]

An enormous number of lamin A/C mutations have been uncovered since the discovery of lamin A/C mutation and its connection with dilated cardiomyopathy.[16] Nearly 500 such mutations in lamin A/C have been reported to date (http://www.umd.be/LMNA/) and these mutations cause muscular dystrophies, lipodystrophies, dilated cardiomyopathy and premature aging syndrome affecting multiple organs.[10,17,18] On the other hand, lamin B1 duplication was shown to produce autosomal dominant leukodystrophy.[19] Interestingly, the recent work from Cristofoli *et al.* has linked for the first time the role of missense mutations in LMNB1 with severe autosomal dominant microcephaly.[20] This has led to a major impetus of research activities focussing primarily on the mutations of lamin A/C and their consequent effects in cells and tissues. It is important to note that almost 15% of the total number of mutations in lamin A/C map in the Ig-fold domain[10] which implies that almost 75% of the amino acid residues in this domain is mutated to missense mutations. This makes it an interesting domain to delve into and address the structural

[a]*Biophysics & Structural Genomics Division, Saha Institute of Nuclear Physics, A CI of Homi Bhabha National Institute, 1/AF Bidhannagar, Kolkata, 700064, West Bengal, India. E-mail: kaushik.sengupta@saha.ac.in*

[b]*Computational Science Division, Saha Institute of Nuclear Physics, A CI of Homi Bhabha National Institute, 1/AF Bidhannagar, Kolkata, 700064, West Bengal, India. E-mail: dhananjay.bhattacharyya.retd@saha.ac.in*

† Electronic supplementary information (ESI) available. See DOI: https://doi.org/10.1039/d2ra05620h

‡ Authors contributed equally.

perturbations associated thereof. Most of these mutations cause Emery Dreifuss Muscular Dystrophy (EDMD), Limb-Girdle Muscular Dystrophy (LDMD) and Dilated Cardiomyopathy (DCM) (http://www.umd.be/LMNA/). We have focussed on three such deleterious mutations R453W, W498C and W498R to check their structural plasticity and the overall effect on the morphology of the nucleus. Out of these 3 mutants, 66 patients with severe phenotypes have been reported to be afflicted by R453W with an early onset. R453W abrogates the two important salt bridges formed by Glu 443 and Glu 444 thereby favouring the transition to unfold rather easily.[4] R453W causes EDMD which is characterized by rigidity of the spine, scapular weakness, contractures of elbows and Achilles' tendons, progressive muscle wasting with frequent cardiac involvement.[21] W498C was shown to produce LGMD1B in the patients who complained of limb-girdle weakness with special emphasis on pelvic girdle. The tryptophan at 498 is located at the C-terminal end of strand 6 and occupies the pocket formed by the hydrophobic side chains. Y481 on β-strand 5 is another such hotspot that has also been reported to cause LGMD1B phenotype in patients.[22] W498C also showed abnormalities in Z-disk arrangement in skeletal muscles with concomitant disorganization of desmin, which is known to connect cytoskeleton to the nuclear surface thus perturbing mechanotransduction from cytoskeleton to nucleoskeleton.[23] In retrospect, our group had shown similar perturbation of lamin A–emerin interaction for the mutant R453W and attributed that to modified mechanotransduction in EDMD nuclei.[4] Patients inflicted with W498R were also diagnosed with severe phenotypes of EDMD.[24]

It must be emphasized at this point that structural coordinates of the full length lamin A are not available due to the inherent difficulty in crystallizing intermediate filament proteins which thereby precludes the availability of X-ray or even NMR structure. Consequently, MD simulations with the full-length protein is practically not feasible for proteins like lamins. Therefore, the structural studies on lamin proteins largely dwell on divide-and-conquer approach where separate domains like rods 1A & 2B[25] and Ig-fold[9] have been separately resolved. Over and above, very few studies have been invested to probe residue wise structural fluctuations in the Ig-fold and the consequences thereof. Dialynas *et al.* carried out HSQC-TROSY NMR experiments with G449V, N456I, L489P and W514R[26] which was further extended by a detailed investigation of longitudinal/transverse relaxations in W514R complemented by MD simulations.[10] In the current work, we have compared local dynamics and diffusional flexibility between R453W, W498C and W498R by FCS using full-length EGFP tagged lamin A protein (646 amino acids) and MD simulations on the Ig-fold domain (110 amino acids) separately. Interestingly enough, we found that R453W exhibited maximum flexural dynamicity over other mutants and the wild type protein. We hereby present a novel and interesting insight into the activity of the Ig-fold domain which in turn modulates the diffusional parameters of the full length protein in the nucleoplasm. This has tremendous implication in the rate of formation of the lamin A network and the lamina underneath the INM. Also, this has shed light for the first time on the role of mutant lamin A in the formation of aberrant nuclei thus explaining pathophysiology of the diseases to a greater detail.

Methods

Plasmids and constructs

Full length wild type lamin A (henceforth referred to as wt LA), R453W, W498C and W498R were cloned into pEGFP (Clontech) and/or pRFP (Clontech) by techniques as described earlier.[6,10,27]

Cell lines and transfection

C2C12 (ATCC) was maintained in DMEM (Gibco, USA) supplemented with glucose to a final concentration of 10 mM, penicillin-streptomycin to a final concentration of 1% and Fetal Bovine Serum (FBS) (HiMedia, India) to a final concentration of 10%. Cells were cultured using standard protocol and were maintained at 37 °C under 5% CO_2. Cells in their early passages were allowed to grow to a maximum of 50–60% confluency in coverslips and 35 mm glass bottom dishes. Cells were co-transfected with GFP tagged wt LA/GFP tagged mutated lamin A along with RFP tagged wt LA. 3 μg of total DNA was transfected with Lipofectamine 2000 (Invitrogen, USA) (DNA : Lipo2k = 1 : 1.5) in serum and antibiotic free medium as described earlier.[28] Cells were used for fluorescence imaging after 24 hours of transfection.

Immunofluorescence and confocal imaging

C2C12 cells were co-transfected with EGFP tagged wt LA/EGFP tagged mutant LA along with RFP tagged wt LA. Transfected cells were fixed and stained as described earlier.[27,28] Slides were imaged by Nikon Eclipse Ti-E microscope with Plan Apo VC 100× oil DIC N2 objective/1.40NA/1.515RI with 4× digital magnification and captured by Nikon Eclipse A1R+ resonant scanner. During Z stack imaging, step size of 0.15 μm was maintained over a z depth of 5 μm. Multi line argon ion laser (488 nm laser line for GFP excitation), solid state laser (405 nm for DAPI excitation) and a He–Ne laser (for RFP excitation with 561 nm laser line) were used. During live cell imaging, movement of the speckles were visualised by maintaining live cell conditions in CO_2 independent medium (Gibco, Thermo Fisher, India) for 1 hour with frames captured at intervals of 30 seconds using the Perfect Focus System (PFS) of Nikon Eclipse A1R+ Ti-E confocal system. Z stack images were processed in Ni Element Analysis AR (Version 4.13.00). Pearson Correlation Coefficients (PCC) and van Steensel's cross-correlation functions (CCF)[29] were measured from manually selected regions of interest with the help of JACoP plugin in ImageJ (1.47v). The number of aggregates in the nucleus were also calculated in ImageJ by setting the threshold value to black and white and converting the image to 8 bit and subsequently outlining and calculating the number of particles by the outline tool and the analyze particles tool respectively.

FCS measurements and calculations

The FCS measurements were performed on a Nikon Eclipse TiE Microscope (Nikon, Japan). All the experiments were carried out

at 25 °C on live C2C12 cells plated on 35 mm glass bottomed dish (Nunc, USA) transfected with EGFP tagged wt LA/mutants. Cells were washed off the phenol red of the media and kept in indicator free warm CO_2 independent media (Gibco, USA) before imaging. The methods used for the fluorescence correlation spectroscopy measurement of transfected cells has been described earlier.[30] All the data were stored in a built-in module of PicoQuant named SymPhoTime 64 (version 1.5). Subsequently the data was plotted and presented by using Microsoft Excel (version 2018). The autocorrelation function (ACF) or $G(\tau)$ was obtained using the equations described earlier.[30] Correspondingly the translational diffusion coefficient or the D_i for the experiments could be determined from the ACF curve fittings from the live cell measurements.[30,31]

Western blot

Cells were harvested post 24 hours of transfection for western blot. The pellets were washed, with sterile 1× PBS, and stored in −80 °C till further use. For lysis, the pellet was treated with Mammalian Protein Extraction Reagent (M-PER) (Thermo Scientific, USA) along with 1× protease inhibitor cocktail (PIC). The lysates were stored at −80 °C. Protein concentrations in cell lysates were measured at 595 nm using Bradford assay (Biorad, USA). Proteins were separated using 10% SDS gel electrophoresis and blotted as described earlier.[28]. Primary antibodies used in this study were Rabbit Anti Lamin A (L1293 Sigma Aldrich, USA) in 1 : 500 and Mouse Anti β Actin (Sigma Aldrich, USA) in 1 : 1000 dilutions. Secondary antibody dilution was 1 : 400 for both anti-mouse and anti-rabbit IgG conjugated to Horse Radish Peroxidase (Santacruz, USA). The blots were repeated at least thrice for consistent results.

Molecular dynamics simulations

All-atom MD simulations were carried out for 500 ns under explicit water solvent conditions for WT and its mutants R453W, W498C and W498R. MD simulations were performed at 300 K at the molecular mechanics level implemented in the GROMACS 5.1.3 software package[32] using the CHARMM36 force field.[33] Initial structure of the native Ig-fold domain protein was taken from PDB[34] with PDB ID 1IFR.[9] All systems were soaked in a cubic box of water molecules with dimensions such that the box ends are at least 10 Å away from the solute edges. Further, the systems were subsequently immersed in a box having TIP3P water molecules.[35] Na^+ and Cl^- ions were added further in the systems for neutralizing. The LINCS algorithm[36] was employed to constrain bond lengths. Long-range electrostatic interactions were treated with particle mesh Ewald summation method[37] and a cut off of 12 Å was used for short-range interactions. All the systems were minimized using 1500 steps of steepest descent algorithm to ensure that the system has no steric clashes, inappropriate geometry or structural distortions. All systems were further equilibrated at a constant temperature[38] of 300 K by utilizing the two-step ensemble process (NVT and NPT) for 100 ps.

The final simulations were performed for each system for 500 ns where leap-frog integrator was applied for the time evolution of trajectories at constant pressure[39] and temperature (NPT). The integration time step was set to 2 fs and the trajectories were analysed using built-in programs of GROMACS software package.[32]

The electrostatic surface potential of the proteins was calculated using the APBS plugin tool of PyMOL.

Analysis of MD trajectories

All the trajectory files were analyzed using trajectory analysis module embedded in the GROMACS simulation package, PyMOL (The PyMOL Molecular Graphics System, Version 2.0 Schrödinger, LLC.) and Visual Molecular Dynamics (VMD) software.[40] To assess the convergence of the MD simulations, root mean square deviations (RMSDs) were calculated. The energy minimised structures for MD were used as the reference structures in RMSD calculations. In addition, root mean square fluctuations (RMSFs) were calculated to evaluate the structural flexibilities of proteins. There are a few parallel methods for calculation of RMSFs as dicussed in recent literature.[41,42] In our case, the RMSFs were calculated using the final 100–500 ns trajectories of equilibration MD simulations using the method as given by eqn (1).

$$\mathrm{RMSF}_i = \sqrt{\left(\langle (x_i - \langle x_i \rangle)\rangle^2\right)} \quad (1)$$

where RMSF_i is the Root Mean Square Fluctuation of the i^{th} atom, x_i is coordinates of the i^{th} atom and $\langle x_i \rangle$ is time average position of the i^{th} atom within 100 to 500 ns and the differences $(x_i - \langle x_i \rangle)^2$ are averaged over snapshots during 100 to 500 ns.

Principal component analysis

Principal components analysis (PCA) is an effective tool for extracting the essential information from MD trajectories by filtering global slow motions from local fast motions.[26,38,43,44] PCA is based on diagonalization of the covariance matrix of atomic fluctuations to obtain orthogonal eigenvectors (also called principal modes) and the corresponding eigenvalues. The eigenvalue indicates the magnitude in the direction of the principal mode. The principal components (PCs) are the projections of a trajectory on the principal modes, of which usually the first few ones are largely responsible for the most important motions. In this work, to detect the conformational change of wild type (WT), R453W, W498C and W498R mutant, PCA was also performed with the GROMACS software package.[32]

Dynamic cross-correlation map (DCCM)

DCCM analysis was performed to evaluate the dynamic correlations of domains and compare the correlation matrix across all Cα atoms for all the systems. The normalized correlation coefficient C_{ij} between two atoms i and j during the course of the simulation trajectory is defined as by eqn (2):[45,46]

$$C_{ij} = \frac{\langle (x_i - \langle x_i \rangle)(x_j - \langle x_j \rangle)\rangle}{\langle x_i - \langle x_i \rangle\rangle^{1/2} \langle x_j - \langle x_j \rangle\rangle^{1/2}} \quad (2)$$

where displacement vectors Δr_i or Δr_j are calculated by subtracting the instantaneous position of i^{th} or j^{th} atoms with its average position. $C_{ij} > 0$ represents the positively correlated motions between the i^{th} and j^{th} atom and $C_{ij} < 0$ represents the negatively correlated motions between them. Dynamic cross-correlation map (DCCM) analysis was performed using Bio3D.[47]

Results

Anomalous assembly and dynamics of lamin A mutants

We had shown earlier that overexpression of mutant lamin A in C2C12 cells led to aggregation throughout the nucleoplasm,[6,10,19,48,49] irrespective of the position of the mutation along the length of the protein. In our present work, we have analysed the differential pattern of assembly of wild type full-length lamin A protein and its mutants (R453W, W498C, W498R) inside the cell. The point mutations under study are localized in the Ig-fold domain and have been depicted in a cartoon (Fig. 1A). Considering the heterozygosity of the mutants, we have co-transfected the cell lines with EGFP tagged lamin A constructs (wt/mutant) and RFP tagged wt LA as shown earlier[31,50] and performed Z-stack imaging of the fixed cell samples to analyse the three-dimensional distribution of the fluorescent proteins throughout the entire volume of the nucleus. The rationale behind this approach is to mimic the effect of the mutant allele on the wild type and its consequence on the formation of lamina.

In the first case where the cells were transfected with both EGFP and RFP tagged wt LA proteins, we observed uniform and intact lamina formation from the 3D distribution of LA which recapitulated the usual characteristic organization of endogenous wt LA underneath the INM. The distribution of LA was continuous and uniform across the entire Z depth (Fig. 1B). However, when the cells were co-transfected with each of EGFP tagged mutant LA (R453W/W498R/W498C) and RFP tagged wt LA, overexpression mediated aggregation of mutant proteins could be observed concomitantly with the formation of a broken nuclear rim (Fig. 1B). The discontinuity in the nuclear rim and abnormal punctate distribution of LA across the Z depth was noticed due to aggregate formation in the mutants (Fig. 1B). Comparatively stable and higher number of aggregates were found in lamin R453W (Fig. 1B). 90–95% of the positively transfected cells showed a similar phenotype for each of the individual mutants.

The RFP tagged wt LA was always found to be sequestered by the mutant aggregates (Fig. 2A). Ectopic expression of the wt LA along with the mutant protein confirmed the sequestration event which was evident from co-localization of the two. Higher numbers of such aggregates were observed for lamin R453W with a PCC value of 0.98 followed by W498C and W498R with

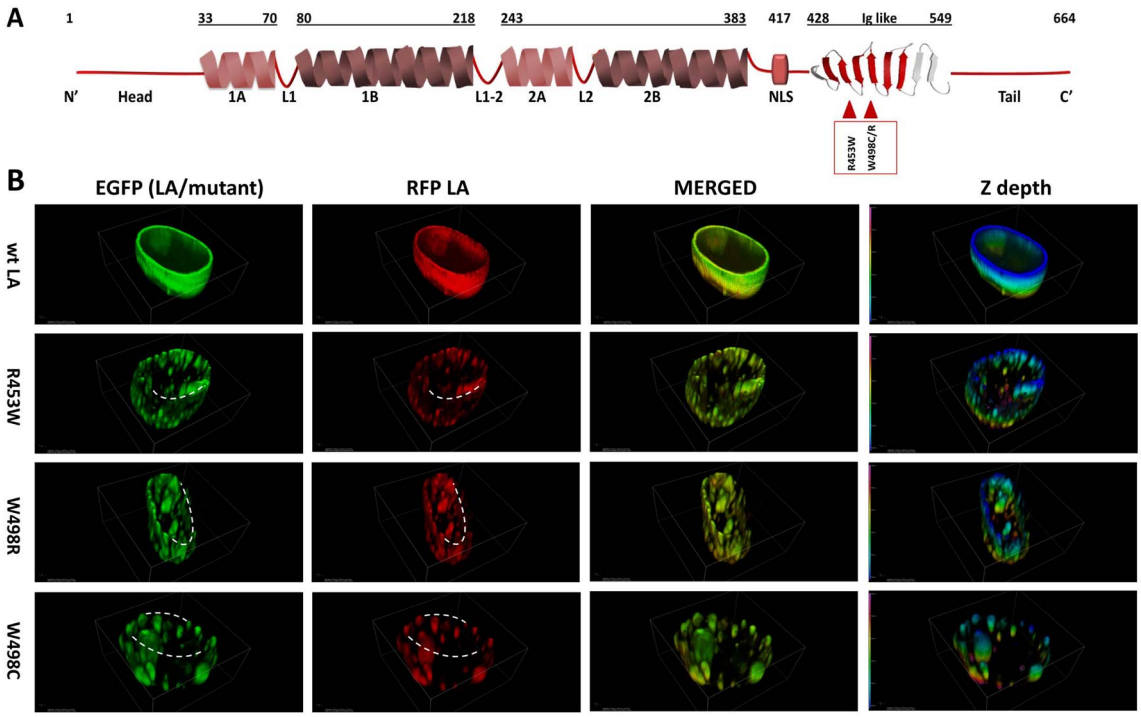

Fig. 1 Abnormal nuclear morphology induced by lamin A mutants. (A) Schematic of lamin A protein indicating the location of point mutations on the Ig-fold studied in this report. (B) C2C12 cells were transiently co-transfected with RFP wt LA and GFP WT/R453WLA/W498CLA/W498RLA. Post 24 hours of transfection, cells were fixed and stained and each nucleus was scanned for a Z depth of 5 μm 3D reconstitution of images along *Z* axis showed a continuous and uniform distribution of lamin A in wt LA whereas all three mutants produced punctate lamina with irregular distribution across the z depth. Comparatively stable and higher number of aggregates were found in R453W. The last panel exhibits the pseudo-colored 3D z depth rendered basal, apical and side views of the nuclear rim indicating an uneven distribution of the aggregates and differences in their size and pattern. Dotted lines show the region where the nuclear lamina is broken.

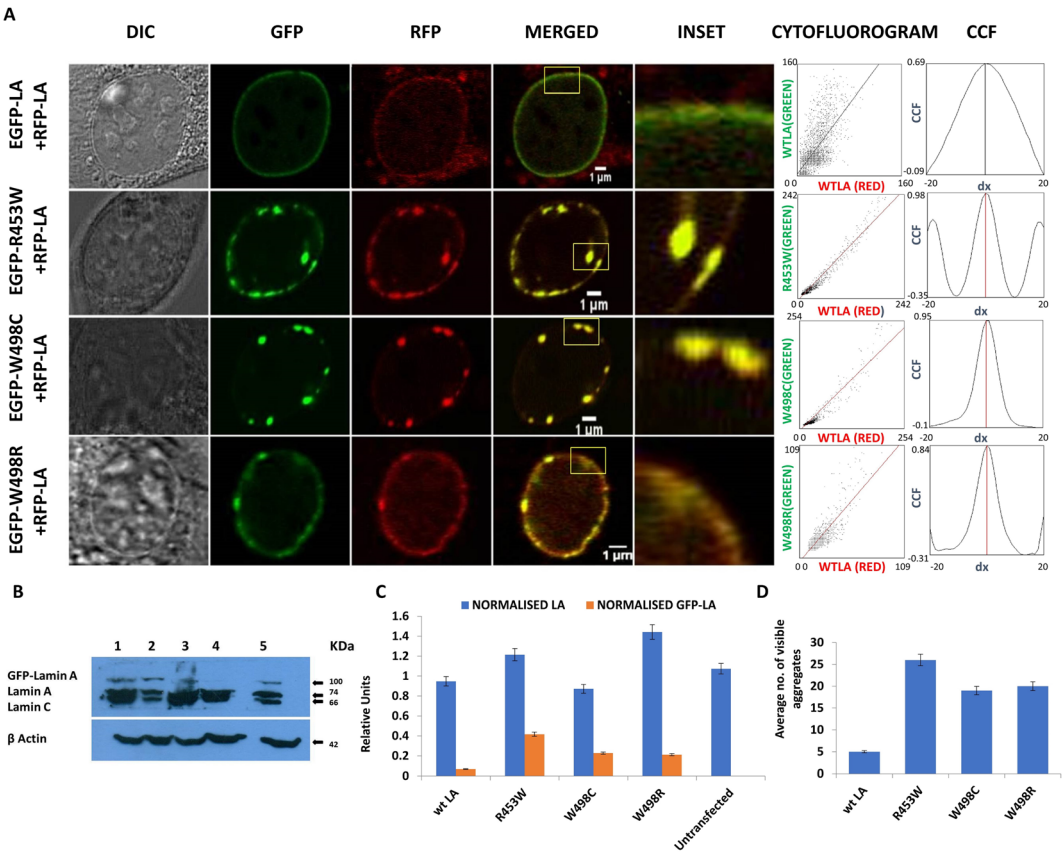

Fig. 2 Sequestration of RFP LA by the mutant aggregates: (A) live cells were imaged for 1 hour. One frame from wt LA and each of the mutants has been selected to show the pattern of speckle formation. Insets of the panels are showing sequestration of GFP tagged WT and mutant lamin A proteins with RFP tagged wt LA in forms of yellow aggregates. PCC values from respective cytofluorograms and van Steensel's cross correlation functions are showing positive correlations in all four co transfection scenario and higher PCC values in the mutant counterparts are indication of stronger association of red and green probes in the yellow aggregates delineated with the ROI shown in the inset. Magnification: 100×. Scale Bar: 1 µm. (B) Western blot showing prominent band of lamin A tagged with EGFP (100 kDa) along with bands for endogenous lamin A/C (74 kDa/66 kDa). (C) Lysates from transfected cells were immunoblotted using Anti Lamin A antibody to check for EGFP LA expressions. 1-R453W, 2-W498C, 3-W498R, 4-non-transfected, 5 wt LA. β Actin (42kDa) is used as loading control (D) The average number of visible aggregates observed in the nucleoplasm for wt LA and the mutants. Error bars indicate percentage error.

PCC values 0.95 and 0.84 respectively. On the other hand, the co-expression of the wt LA with RFP and GFP fluorophore resulted in a few small puncta with a PCC value of 0.69 which is common in all ectopic expression scenario (Fig. 2A). Higher PCC values in the mutant proteins indicate a greater correlative variation of GFP tagged mutant lamin A along with RFP tagged wt LA. The fact that the phenotypes observed for the mutants didn't result from expression artefact but were true effects due to the mutations, was corroborated from the expression profile of the proteins in western blot (Fig. 2B) which was quantified (Fig. 2C). On quantification, largest number of aggregates were observed for R453W (~25) while lowest for wt LA (not more than 5) (Fig. 2D).

To summarize these observations, we conclude that these mutations showed a preponderance of non-specific anomalous aggregation over stepwise assembly into an intact lamina. The aggregates of varying sizes acted as "sequestration sinks" which are in stark contrast to the wild type which predominantly formed an intact lamina along with some small aggregates. In R453W aggregates, greater spatial correlation of red and green fluorescent probes was observed with respect to the other two mutants depicting higher proportional co-distribution of the two fluorescent proteins. The van Steensel's cross correlation function suggests how the PCC alters as a function of the shift of red image pixel to green. Peaks at the centre in CCF plots for all three mutants as well as WT variety depict that the fluorescent signals from the two channels in the mutants and the wild type were all positively correlated but to different extents.

We also observed differential mobility of the mutant aggregates with infinitesimally small movements for the wt LA (ESI video S1†). Since there were minute or no translational artefacts of living cells on the glass plate over 3600 seconds, the observations were not processed further to draw any significant conclusions (ESI video S1†). To summarize the results obtained, we invoke a model to explain the abnormal ability of the mutants to form non-specific aggregates following a course of random association rather than exhibiting a slow, systematic and stepwise assembly to a functional lamina of giant polymeric structure and almost zero dynamicity. This prompted us to analyse the diffusional flexibility of the full-length proteins *in*

vivo by fluorescence correlation spectroscopy and later on to study the mobility of the very specific domain harbouring the mutations in a more precise manner by molecular dynamic simulations.

Differential diffusional parameters of mutant lamin A proteins in the nucleoplasms

It is well established from earlier studies that the nuclear lamina has lamin proteins having little or no mobilities but the soluble fraction of lamin A proteins are mobile and the diffusion parameters have also been well characterized earlier by FRAP[51] and subsequently with the help of FCS in a number of studies.[31,52,53] Therefore, taking cues from those studies, we have compared the diffusional motions of full length lamin A and its 3 mutants by employing FCS based microscopy technique whereby we get information on their diffusivity and dynamics with single molecule sensitivity (Fig. 3) in femtolitre volume. Fluorescence intensity fluctuations in the nucleoplasm of transiently transfected live C2C12 cells expressing GFP tagged wild type and mutant Lamin A were recorded individually at 24–48 h after transfection. A typical C2C12 cell expressing wild type lamin A is shown (Fig. 3A). Cells expressing GFP-tagged proteins were localized by confocal imaging and the position of the confocal detection volume was assigned at arbitrary locations in the nucleoplasm, carefully avoiding the aggregated proteins corresponding to increased brightness in case of the mutants.

Measuring time was set to 10 s as described earlier[30] which was appropriate to obtain reliable autocorrelation functions. Representative photon count rate records, measured with FCS, from EGFP-LA and mutants in the nucleoplasm (Fig. 3B) are shown. For comparison of the mobility, the amplitude of $G(\tau)$ ($G(0) - 1$) was normalized to 1.

W498C exhibited slightly faster diffusivity followed by the wild type and W498R which were almost similar whereas the slowest value was recorded for R453W (Fig. 3C). The diffusion constants of the full length lamin wt LA and the mutant LAs are summarized in the table (Fig. 3D). It must be emphasized that the slow and fast diffusivity obtained from the two-component analysis correspond to a slow mobile fraction and a fast mobile fraction as described earlier.[30,31,52,54,55] This points to the fact that R453W diffuses rather slowly which could be due to an increase in its bulk. This is in good agreement with our previous observation with SMFS where R453W was found to unfold at a lower force compared to the Ig fold domain of wild type.[4] We conjectured that this differential diffusional dynamics of the full length protein could be a direct consequence of the microdynamics of the Ig fold domain which harbours the mutations. To test this hypothesis, we performed MD simulations of the Ig fold domain subsequently.

Association and dynamics of the Ig-fold

We analysed the electrostatic surface potential and performed MD simulations for 500 ns on the wt and the three mutant Ig-

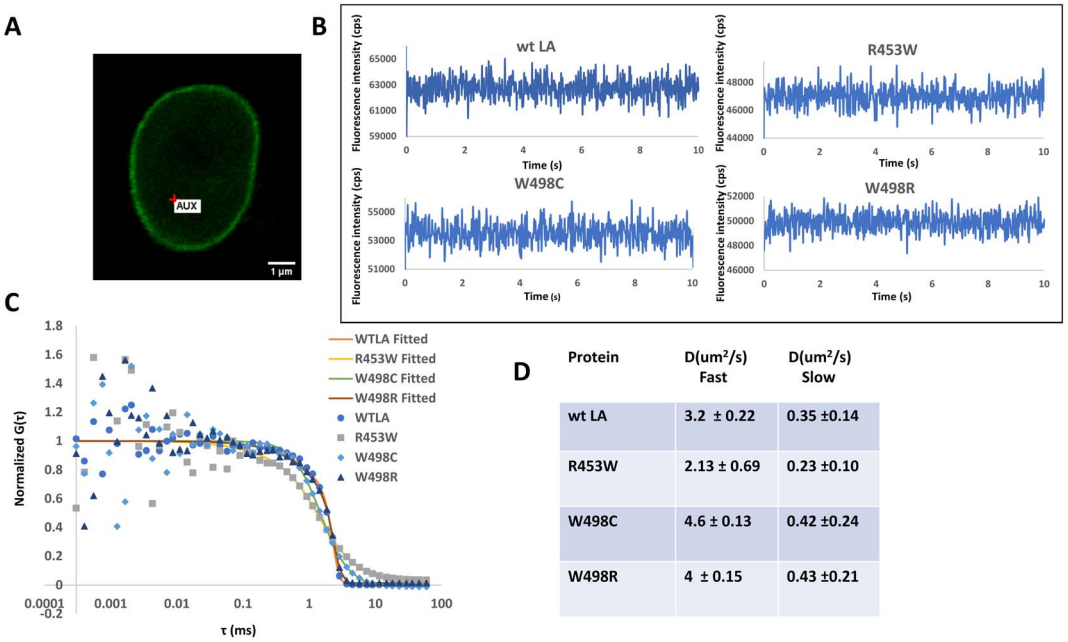

Protein	D(um²/s) Fast	D(um²/s) Slow
wt LA	3.2 ± 0.22	0.35 ±0.14
R453W	2.13 ± 0.69	0.23 ±0.10
W498C	4.6 ± 0.13	0.42 ±0.24
W498R	4 ± 0.15	0.43 ±0.21

Fig. 3 Study of the nucleoplasmic diffusional mobility of wild type and mutant full length proteins *in vivo* by fluorescence correlation spectroscopy: the differential mobilities of wild type GFP lamin A (wt LA), R453W, W498R and W498C in C2C12 cells were analysed by FCS. (A) A representative image of a nucleus expressing wild type GFP lamin A during FCS measurements. The red point indicates the ROI where the measurements were obtained. Scale bar: 1 µm. (B) Representative fluorescence fluctuation of GFP-LA and the mutants in the nucleoplasm has been plotted as a function of time. (C) Averaged fluorescence autocorrelation curves were calculated from the fluorescence intensity fluctuations and plotted as a function of time. $G(\tau)$ is the fluorescence autocorrelation function. For comparing the diffusional mobility, all curves were normalised to the amplitude $G(\tau) = 1$ at 0 seconds. (D) Table displays the fast and slow diffusion coefficients of mutant and wild type full length lamin A proteins in live cells as determined by FCS. The p-value was found to be <0.05 (one-way ANOVA) compared with the wt LA.

fold domains. The structures after 500 ns MD simulations, along with their electrostatic potential surfaces are shown in Fig. 4, which indicates that the mutations didn't result in gross structural perturbations of the protein. The Ig-fold was maintained in each system with its signature β-sheet sandwich. The electrostatic potentials, as calculated by APBS toolkit of PyMOL, however, indicated major changes in electrostatic nature of the protein upon most of the mutations. Presumably, this might perturb its association with other proteins in the cellular environment. The wt Ig-fold shows prominent positive and negative patches respectively near N-terminal (residue 436) and the long loop near 512 which faded out in the R453W and W498C. In case of W498R, another region near N & C termini assumed a highly positive patch. This might lead to an increased tendency of non-specific association for the mutants resulting into aggregates/speckles.

However, the root mean square fluctuations (RMSF) of all the systems indicated that the amplitude of atom displacements was different among the wt and the mutants (Fig. 5A). Most of the residues adopting β-sheet conformations exhibited low RMSF whereas the loop regions showed larger fluctuations with wide variations. For instance, the loop region between the two parallel stranded β-strands (6^{th} and 7^{th}, residues 500 to 515) showed higher fluctuation for most of the mutants and the wild type. The R453W mutant showed highest fluctuations for residues 475 and 525, which remained close to each other in Euclidian space. This is in good agreement with the previous data from Krimm and Justin 2002 (ref. 8) where large fluctuations in chemical environment are detected around solvent exposed cys 522. It may be noted that the site of mutation (453) is quite far from the regions of high fluctuation. The root mean square deviation (RMSD) was monitored during the simulation time to investigate the protein stability. The RMSD values converged very well in all the systems, within 100 ns, thus the MD trajectories from 100–500 ns were chosen for further conformational analyses (Fig. 5B). Mean values of RMSD of the wt, R453W, W498C and W498R system were approximately 1.81–2.34 Å, indicating that the 3D structure of the Ig-folds was stable in all the cases. Similarly, the volume of the system boxes stabilize quickly during the NPT production runs (ESI Fig. 1†). These further indicate that the modelled structures of the mutants can be considered as reasonable models after sufficient NPT equilibration during the 500 ns production runs. Therefore, we speculated that there might be some long-range effect in the otherwise compact protein. The positively charged side-chain of Arg-453 protrudes out towards solvent for

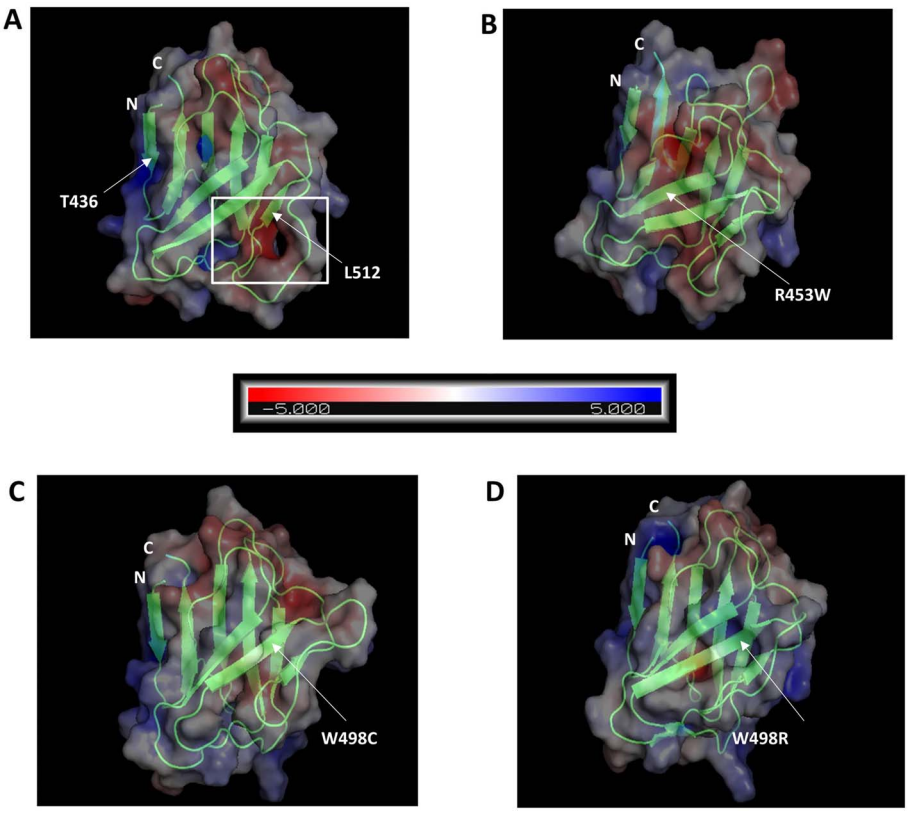

Fig. 4 Electrostatic potential surface potential along with secondary structure of each of the four mutants. (A) WT, (B) R453W, (C) W498C and (D) W498R, showing conservation of secondary structure but reduction in absolute potential polarity for most of the mutants. Scale bar denotes transition from red to blue where red indicates negative potential and blue indicates positive potential. The residues are marked by white arrows while the region of negative potential in the wt which reduces significantly in the mutants is highlighted by a rectangle. The two termini are marked by N and C, respectively for N- and C-terminal amino acids. Scale bar denotes transition from red to blue where red indicates negative potential and blue indicates positive potential (K_bT/e_c).

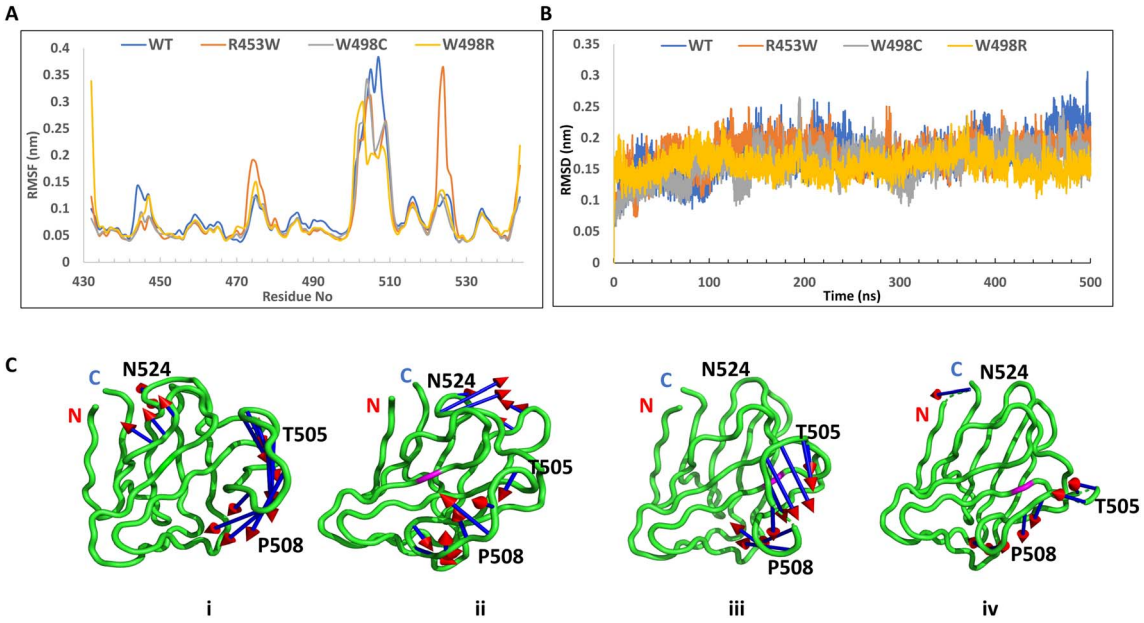

Fig. 5 Dynamics of the Ig-fold proteins by MD simulation. (A) Root Mean Square Fluctuation (RMSF) calculation of Ig-fold proteins. The main difference in structure of the wild type and R453W mutant protein is at the region involving the residues 475 and 525. Color coding – black: WT, red: R453W, green: W498C, blue: W498R. (B) Root mean square deviation of Cα atoms of the four mutant proteins with respect to their respective energy minimized structures. C-alpha Root Mean Square Deviation (RMSD) of Ig-fold protein. All the RMSD values were calculated by using crystal structure as reference and protein Cα atoms for least fitting. (C) Porcupine plot analysis for the proteins. (i) WT (ii) R453W (iii) W498C and (iv) W498R lamin mutants. The arrows indicate the direction of eigenvectors and the length of the arrow represents the magnitude of eigenvalues. For the mutant proteins, pink represents the substituted amino acid. The two termini are marked by N and C, respectively for N- and C-terminal amino acids.

the native protein, which is mutated to hydrophobic Trp, by single nucleotide alteration in the genomic sequence, in the diseased form, which may be accommodated by different ways. The protein might destabilize the third β-strand by pushing the Trp side-chain towards core of the β-sandwich or assume multimeric form by association with other proteins. In our computational study, we cannot simulate protein–protein association but we observed the Trp side-chain remain exposed through long range perturbation. Theoretical studies of protein–protein association require not only advance MD simulation but also protein–protein docking. Rigid body docking between two proteins is very difficult due to size of the macromolecules. In addition, flexibilities of the protein need to be considered as conformations of a free protein and a complex may differ considerably. Thus, a combination of docking and MD simulation is required and such method has not been developed yet.

In this work, PCA analyses were performed to extract the essential dynamical motions by filtering global slow motions from the fast motions for WT, R453W, W498C and W498R systems. The movements along the first principal component (PC1) from PCA analysis is presented in Fig. 5C. The length of cone represents the magnitude of motion and the pointing of the arrow shows the direction. In all the systems fluctuations were observed near the T505 and P508 regions. In R453W, pronounced fluctuations were observed near the G523 & N524 regions when compared to other systems. However, the motions in other regions were absent. Interestingly, it was found that the three proteins, namely WT, W498C and W498R showed similar features in the movements of amino acids near residue numbers 505 (in the loop between 6th and 7th β-strands) with respect to the N and C-terminal regions of the domain. The R453W, however, showed opposite motions of the same residues. This might be again due to loss of the salt-bridge between R453 and E443 side chains.

Backbone & secondary structural analysis

It is a well documented fact that movements of important amino acids within particular secondary structural motifs may alter secondary structures of the whole protein to a certain extent. We have analysed alterations of secondary structures of each amino acid in each mutant using DSSP algorithm[56] to understand such alterations of secondary structures (Fig. 6). Most of the important differences in the backbone flexibility are mainly localized in the vicinity of the mutated residue. In native, the residues around 512 existed as "bend" conformation till the end of the simulation whereas in all mutants this region retained "turns" conformation only. Between the residues 492–495, the wt showed "turn" with traces of "bend", whereas in the mutants primarily "turn" conformation was mainly prevalent. In the 455 residue region, β sheet conformation was observed throughout the simulation time in wt, whereas in mutant "turn" was getting disrupted and attained coil conformation. To summarize this part, very slight changes in secondary structure conformation was observed in the WT and the mutants. A few

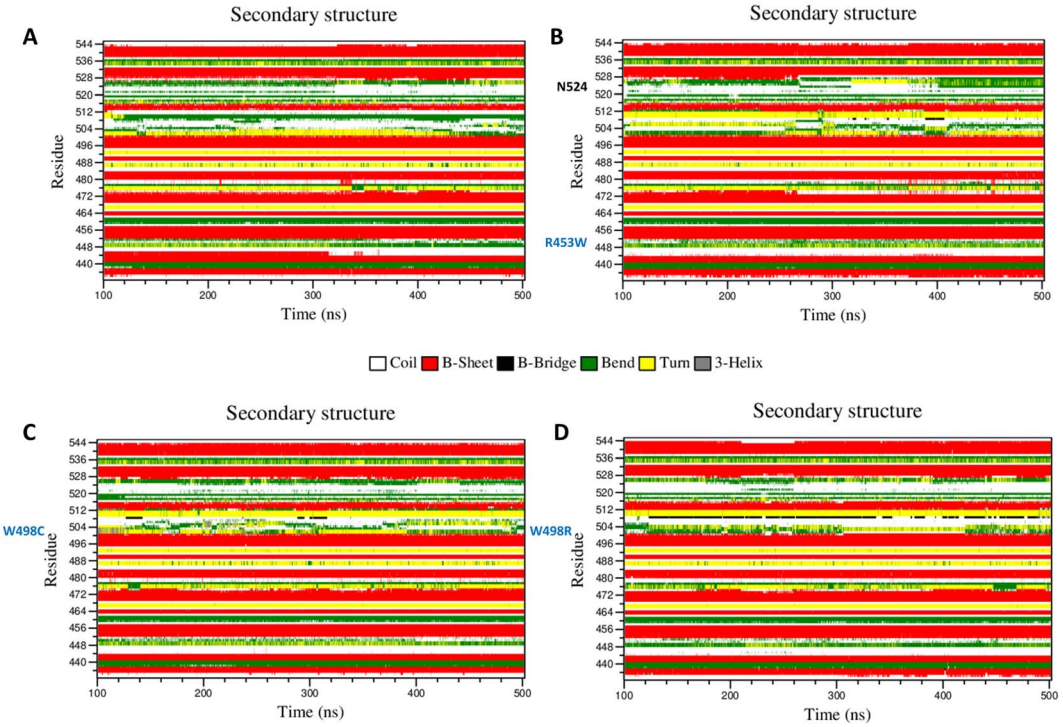

Fig. 6 Spatio-temporal variation of secondary structures of the proteins during simulation. (A) WT, (B) R453W, (C) W498C and (D) W498R. Alteration of secondary structures of the different residues (as *y* axis) of the four proteins during the last 400 ns (as *x* axis) MD simulations, as identified by DSSP algorithm, are shown here. The residues of the lamin A ig fold domain and its mutants can adopt various secondary structures such as coil (white), beta sheet (red), beta bridge (black), bend (green), turn (yellow) and 3_{10} helix (grey). The locations of the mutated residues are highlighted by blue while the maximally flexible residue on R453W mutant is indicated by black.

residues near Ser-525 of the R453W mutant showed alteration of structural features. These alterations are results of multi-modal distributions of φ and ψ torsion angles. In the R453W mutant, Glu-443 showed unusual fluctuations in its φ and ψ torsion angles due to abrogation of the salt bridge between Glu-443 and Arg-453 present in the wild type.

Dynamic cross-correlation matrix (DCCM)

As we found altered motions of some of the residues far from the points of mutations, it appears that the structural cue of the mutations might be transferred through the secondary structural elements by some consorted motions. We have thus characterized the correlated motions between residues of wt LA and the mutant proteins (Fig. 7). The dynamic cross-correlation matrix was used to identify the correlated motions and communications between different residues. Correlated motions were extracted in domains of the structures, and normalized to [−1, 1]. The negative values of DCCM represent the functional displacement of Cα atoms in the opposite direction and *vice versa*. The DCCM map is symmetrical, and the diagonal values, corresponding to correlation between every i^{th} and $(i + 1)^{th}$ amino acid, represent the maximum correlation. We hypothesize that the close emergence of positive and negative correlated motions makes the domain less stable. We observed high anti-correlation in the native structure compared to mutant structures indicating a more compact structure of the wild type. The positive correlation between residues of β-strands 3^{rd}, 6^{th} and those of 4^{th}, 5^{th} indicates a passage of dynamics across the two β-sheet planes. It may be noted that the loop regions consisting of residues 457–467 and 483–493 have some β-sheet property, indicating these pairs of strands had some continuity. This mode of extended β-sheet or β-helix like property was prominently visible in the wild type.

Discussions

The Ig-fold domain of lamin A has important implications in deciphering the pathophysiology of laminopathies as it is a mutational hotspot. The availability of X-ray and NMR structures[8,9] has spearheaded active research into structural perturbation upon the introduction of mutations. Ig-fold domain of lamin A consists of nine β-strands. The sheet of five β strands, 1, 4, 5, 8, and 9 make an angle of 45° with another sheet comprising of 4 strands 2, 3, 6, and 7 thus making up a characteristic β sandwich structure.[4,8,9] Previous reports had proven the abolition of beta bulge due to the mutation R453W where the salt bridges with Glu 443 and Glu 444 are abrogated thus facilitating the route for unfolding.[4] The same was also proven by steered molecular dynamics and single molecular force spectroscopy. As a consequence of this structural alteration, we had also observed the aberrant self-association behaviour of the mutant protein due to its electronegative surface potential.[4]

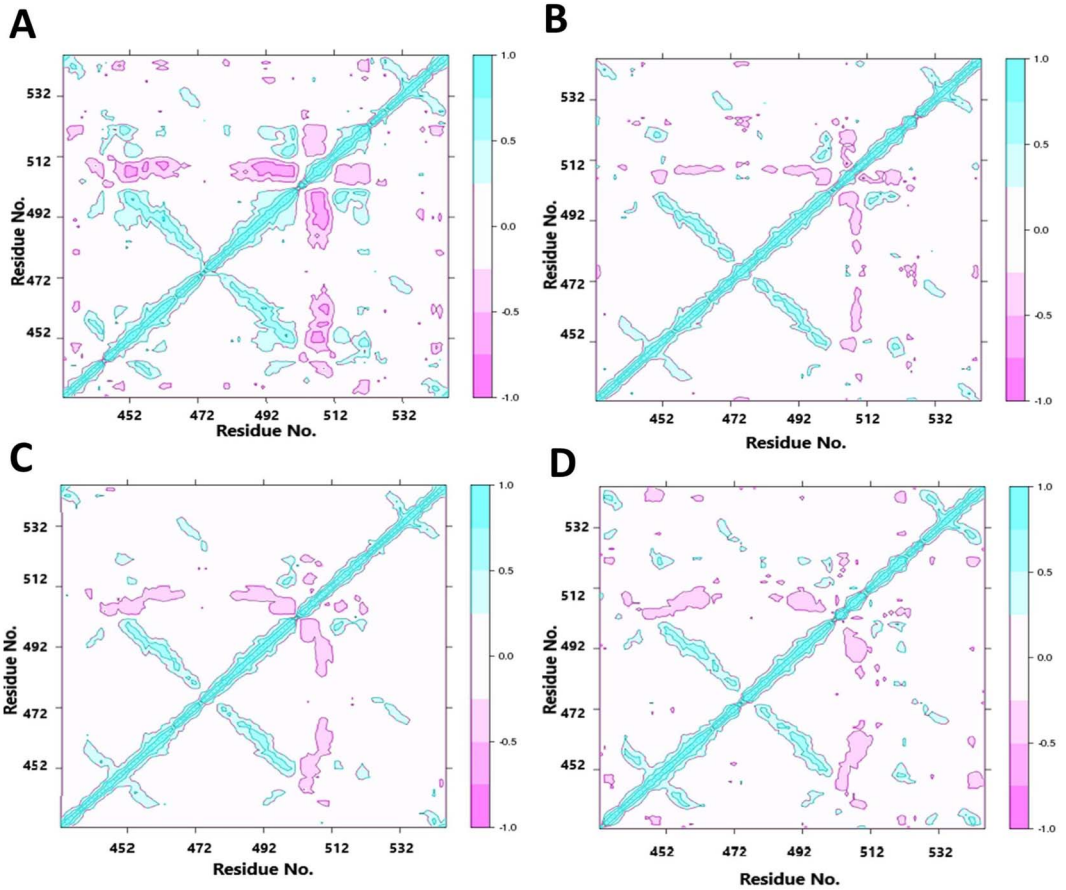

Fig. 7 Dynamic cross-correlation matrices of the proteins (A) WT, (B) R453W, (C) W498C and (D) W498R proteins. Cyan represents a positive correlation and pink represents a negative correlation. The color gradient represents the gradual decrease in the correlation.

In addition to these earlier findings, (a) we have made in-depth analyses of this protein along with two other mutants W498R & W498C both inside the cell and (b) *in silico* by MD simulations on the Ig-fold domain. We have visualized formation of misshapen and aberrant nuclei in the case of these mutants when we overexpressed the proteins in cells. Formation of normal, continuous lamina was abrogated by aggregates of varying sizes and numbers. Ectopic expression of R453W produced smaller and numerous aggregates whereas W498R/C produced slightly larger aggregates but fewer in number. Live cell tracking of translational motions of these aggregates could not provide noticeable differences due to their restricted mobility.

We refined our analysis through (c) FCS by focussing on diffusional motions into very small volumes inside the nucleoplasm where visible aggregates were absent. Interestingly enough, we obtained small diffusion coefficient and consequently longer diffusional times for R453W compared to the wt LA and W498R/C. We interpreted this result as a contribution of motion of a more voluminous molecule with concomitant longer diffusion times. We could thus explain that the appearance of numerous visible aggregates for R453W which might have resulted from frequent non-specific and anomalous association between the protein molecules in an ensemble. Now the obvious question was why R453W seeded the formation of a greater number of macromolecular structures. Along this line of observation, we reasoned that the microdynamics of the Ig fold domain might hold the answer to this question. In the case of R453W, the observed RMSF from our MD simulations over 500 ns, predicted higher fluctuations resulting in higher unbalanced forces. The fluctuations occurring throughout the Ig-fold domain has been depicted by the eigenvectors. It is hypothesized that this domain exhibits faster stochastic movements leading to a higher preponderance of random self-association to form aggregates thereby lowering the probability of a stepwise steady association.

It must be emphasized here that previous work has already established the likelihood of overlap of the tail domain containing the Ig fold on the rod domains to completely define this structure of full length lamin A. This study had convincingly proved the perturbation of the electronic environment of the tryptophan residues in the Ig fold domain as a sequel to mutations in the rod domain.[6] Therefore, from the current study it can be conjectured that alteration in microdynamics of the Ig fold domain due to the mutations thereof would certainly modulate the overall dynamics of the full length protein in some way or the other which in turn would affect the process of association of lamin A oligomers through a stepwise assembly

process originating from dimer.[57] The rationale of our explanation is in excellent agreement with a previous report where the researchers focussed on MD simulation of a specific VWF A2 domain (356 aa) of von Willebrand Factor protein (2813 aa) and concluded the corresponding effects on the dynamics, oligomerisation, and enzymatic action of the full length protein.[58] Recent studies with DEAD-Box Helicase 3 X-Linked protein showed identical results with respect to protein hyper assembly based aggregation and sequestration of healthy proteins, thereby abrogating normal cell function.[59] Taken together, we can conclude that changes in local dynamics of a domain could indeed reflect in the molecular assembly process of a protein like lamin A. Hence, we can explain the formation of broken lamina and misshapen nuclei in the case of the mutants with a more pronounced effect in the case of R453W. This can explain the severe phenotypes associated with R453W afflicted patients of autosomal dominant EDMD.

The other mutants W498R & W498C also showed fluctuations similar to R453W but lower in magnitude which was corroborated by lower RMSF values comparable to the wild type protein. Slower fluctuations would lower the rate of random association thereby producing less bulky species with higher rates of diffusion as observed from FCS. To summarize our observations, we state that the microdynamics of the Ig fold domain plays a decisive role in the stepwise lamina assembly. This is reminiscent of our observations[6] where we had predicted a partial overlap of the tail domain with a portion of the rod domain. The Ig fold thus being in the C-terminal domain could potentially exert its influence on the homooligomerization of the protein which principally occurs along the coiled-coil rod domain (residues 30–386). Therefore, any change in microdynamics of the Ig fold containing C-terminal domain could adversely affect the process of stepwise synchronized assembly into a higher order functional lamina. We hypothesize for the first time that AD-EDMD and other muscular dystrophies associated with R453W and W498R/C which are largely characterized by aberrant nuclei and broken lamina could very well be caused by such abnormal dynamics of Ig fold domain. This opens the avenues for further investigations into the dynamics of individual domains of the protein and the effect on molecular assembly.

Conclusion

(1) Formation of misshapen and aberrant nuclei was visualized when the mutant proteins were expressed in the cells.

(2) R453W produced smaller and numerous aggregates whereas W498R/C produced slightly larger aggregates but fewer in number.

(3) Longer diffusional times for R453W compared to the wt LA and W498R/C was observed.

(4) In the case of R453W, the observed RMSF from MD simulations predicted higher fluctuations resulting in higher unbalanced forces.

(5) As a consequence, microdynamics of the Ig fold domain plays a decisive role in the stepwise lamina assembly.

Funding

CM, DS thank DAE, Govt. of India for the fellowship. LM thanks NPDF, SERB, DST, Govt. of India. DB thanks APP2, DAE, Govt. of India. KSG thanks SERB, DST & BARD project of DAE, Govt. of India.

Data availability

All representative data generated or analysed during this study are included in this submitted article and its ESI files.† The total datasets generated during and/or analysed during the current study are available from the corresponding author on reasonable request. No mandated datasets having information or access links are used in this paper. However, the details of molecular dynamic simulation based on GROMACS and CHARMM platforms can be provided as and when required.

Conflicts of interest

The authors declare no conflict of interest.

Acknowledgements

CM, DS, LM & M. M. performed the experiments. CM, DS, LM, DB & KSG wrote the manuscript. The project was conceived by KSG.

References

1 D. Z. Fisher, N. Chaudhary and G. Blobel, *Proc. Natl. Acad. Sci. U. S. A.*, 1986, **83**, 6450–6454.
2 F. D. McKeon, M. W. Kirschner and D. Caput, *Nature*, 1986, **319**, 463–468.
3 M. N. Guilly, A. Bensussan, J. F. Bourge, M. Bornens and J. C. Courvalin, *EMBO J.*, 1987, **6**, 3795–3799.
4 M. Bera, H. C. Kotamarthi, S. Dutta, A. Ray, S. Ghosh, D. Bhattacharyya, S. R. Ainavarapu and K. Sengupta, *Biochemistry*, 2014, **53**, 7247–7258.
5 S. V. Strelkov, J. Schumacher, P. Burkhard, U. Aebi and H. Herrmann, *J. Mol. Biol.*, 2004, **343**, 1067–1080.
6 P. Bhattacharjee, A. Banerjee, D. Dasgupta and K. Sengupta, *Biochemistry*, 2013, **52**, 4229–4241.
7 E. C. Schirmer, T. Guan and L. Gerace, *J. Cell Biol.*, 2001, **153**, 479–489.
8 I. Krimm, C. Ostlund, B. Gilquin, J. Couprie, P. Hossenlopp, J. P. Mornon, G. Bonne, J. C. Courvalin, H. J. Worman and S. Zinn-Justin, *Structure*, 2002, **10**, 811–823.
9 S. Dhe-Paganon, E. D. Werner, Y. I. Chi and S. E. Shoelson, *J. Biol. Chem.*, 2002, **277**, 17381–17384.
10 S. Dutta, J. K. Das, L. Maganti, M. Bhattacharyya, D. Bhattacharyya, S. Mukherjee and K. Sengupta, *Sci. Rep.*, 2018, **8**, 13793.
11 C. A. Glass, J. R. Glass, H. Taniura, K. W. Hasel, J. M. Blevitt and L. Gerace, *EMBO J.*, 1993, **12**, 4413–4424.
12 E. C. Schirmer and R. Foisner, *Exp. Cell Res.*, 2007, **313**, 2167–2179.

13 T. Dechat, K. Pfleghaar, K. Sengupta, T. Shimi, D. K. Shumaker, L. Solimando and R. D. Goldman, *Genes Dev.*, 2008, **22**, 832–853.
14 D. K. Shumaker, L. Solimando, K. Sengupta, T. Shimi, S. A. Adam, A. Grunwald, S. V. Strelkov, U. Aebi, M. C. Cardoso and R. D. Goldman, *J. Cell Biol.*, 2008, **181**, 269–280.
15 T. Moriuchi, M. Kuroda, F. Kusumoto, T. Osumi and F. Hirose, *Exp. Cell Res.*, 2016, **342**, 83–94.
16 D. Fatkin, C. MacRae, T. Sasaki, M. R. Wolff, M. Porcu, M. Frenneaux, J. Atherton, H. J. Vidaillet, Jr., S. Spudich, U. De Girolami, J. G. Seidman, C. Seidman, F. Muntoni, G. Muehle, W. Johnson and B. McDonough, *N. Engl. J. Med.*, 1999, **341**, 1715–1724.
17 K. H. Schreiber and B. K. Kennedy, *Cell*, 2013, **152**, 1365–1375.
18 H. J. Worman, C. Ostlund and Y. Wang, *Cold Spring Harbor Perspect. Biol.*, 2010, **2**, a000760.
19 P. Bhattacharjee, D. Dasgupta and K. Sengupta, *J. Phys. Chem. B*, 2015, **119**, 14014–14021.
20 F. Cristofoli, T. Moss, H. W. Moore, K. Devriendt, H. Flanagan-Steet, M. May, J. Jones, F. Roelens, C. Fons, A. Fernandez, L. Martorell, A. Selicorni, S. Maitz, G. Vitiello, G. Van der Hoeven, S. A. Skinner, M. Bollen, J. R. Vermeesch, R. Steet and H. Van Esch, *Am. J. Hum. Genet.*, 2020, **107**, 753–762.
21 E. Mercuri, S. C. Brown, P. Nihoyannopoulos, J. Poulton, M. Kinali, P. Richard, R. J. Piercy, S. Messina, C. Sewry, M. M. Burke, W. McKenna, G. Bonne and F. Muntoni, *Muscle Nerve*, 2005, **31**, 602–609.
22 S. Spuler, C. Geier, K. J. Osterziel, M. Gutberlet, J. Genschel, T. N. Lehmann, S. Zinn-Justin, B. Gilquin and H. Schmidt, *J. Neurol.*, 2005, **252**, 621–623.
23 A. D'Amico, S. Benedetti, S. Petrini, N. Sambuughin, R. Boldrini, I. Menditto, M. Ferrari, M. Verardo, L. Goldfarb and E. Bertini, *Neuromuscular Disord.*, 2005, **15**, 847–850.
24 M. Pasotti, C. Klersy, A. Pilotto, N. Marziliano, C. Rapezzi, A. Serio, S. Mannarino, F. Gambarin, V. Favalli, M. Grasso, M. Agozzino, C. Campana, A. Gavazzi, O. Febo, M. Marini, M. Landolina, A. Mortara, G. Piccolo, M. Vigano, L. Tavazzi and E. Arbustini, *J. Am. Coll. Cardiol.*, 2008, **52**, 1250–1260.
25 S. V. Strelkov, H. Herrmann, N. Geisler, T. Wedig, R. Zimbelmann, U. Aebi and P. Burkhard, *EMBO J.*, 2002, **21**, 1255–1266.
26 G. Dialynas, O. K. Shrestha, J. M. Ponce, M. Zwerger, D. A. Thiemann, G. H. Young, S. A. Moore, L. Yu, J. Lammerding and L. L. Wallrath, *PLoS Genet.*, 2015, **11**, e1005231.
27 P. Bhattacharjee, D. Dasgupta and K. Sengupta, *Biochim. Biophys. Acta, Gen. Subj.*, 2017, **1861**, 2598–2608.
28 C. Mukherjee, A. Kundu, R. Dey, A. Banerjee and K. Sengupta, *Soft Matter*, 2021, **17**, 6787–6796.
29 S. Bolte and F. Cordelières, *J. Microsc.*, 2006, 224.
30 S. Takeshi, C. G. Pack and R. D. Goldman, *Methods Mol. Biol.*, 2016, **1411**, 99–111.
31 V. Kochin, T. Shimi, E. Torvaldson, S. A. Adam, A. Goldman, C. G. Pack, J. Melo-Cardenas, S. Y. Imanishi, R. D. Goldman and J. E. Eriksson, *J. Cell Sci.*, 2014, **127**, 2683–2696.
32 M. J. Abraham, T. Murtola, R. Schulz, S. Páll, J. C. Smith, B. Hess and E. Lindahl, *SoftwareX*, 2015, **1–2**, 19–25.
33 P. Bjelkmar, P. Larsson, M. A. Cuendet, B. Hess and E. Lindahl, *J. Chem. Theory Comput.*, 2010, **6**, 459–466.
34 H. M. Berman, J. Westbrook, Z. Feng, G. Gilliland, T. N. Bhat, H. Weissig, I. N. Shindyalov and P. E. Bourne, *Nucleic Acids Res.*, 2000, **28**, 235–242.
35 W. Jorgensen, J. Chandrasekhar, J. Madura, R. Impey and M. Klein, *J. Chem. Phys.*, 1983, **79**, 926–935.
36 B. Hess, H. Bekker, H. J. C. Berendsen and J. G. E. M. Fraaije, *J. Comput. Chem.*, 1997, **18**, 1463–1472.
37 T. Darden, D. York and L. Pedersen, *J. Chem. Phys.*, 1993, **98**, 10089–10092.
38 B. L. de Groot, A. Amadei, R. M. Scheek, N. A. J. van Nuland and H. J. C. Berendsen, *Proteins: Struct., Funct., Bioinf.*, 1996, **26**, 314–322.
39 M. Parrinello and A. Rahman, *J. Appl. Phys.*, 1981, **52**, 7182–7190.
40 W. Humphrey, A. Dalke and K. Schulten, *J. Mol. Graphics*, 1996, **14**(33–38), 27–38.
41 A. Diez Fernandez, P. Charchar, A. G. Cherstvy, R. Metzler and M. W. Finnis, *Phys. Chem. Chem. Phys.*, 2020, **22**, 27955–27965.
42 D. L. Z. Caetano, R. Metzler, A. G. Cherstvy and S. J. de Carvalho, *Phys. Chem. Chem. Phys.*, 2021, **23**, 27195–27206.
43 J. Hu and C. Wang, *Chin. J. Chem.*, 2010, **28**, 33–40.
44 S. Chang, J.-p. Hu, P.-y. Lin, X. Jiao and X.-h. Tian, *Mol. BioSyst.*, 2010, **6**, 2430–2438.
45 J. A. McCammon, *Rep. Prog. Phys.*, 1984, **47**, 1–46.
46 B. B. Smith, *Biochem. Educ.*, 1989, **17**, 220.
47 L. Skjærven, X.-Q. Yao, G. Scarabelli and B. J. Grant, *BMC Bioinf.*, 2014, **15**, 399.
48 A. Banerjee, V. Rathee, R. Krishnaswamy, P. Bhattacharjee, P. Ray, A. K. Sood and K. Sengupta, *PLoS One*, 2013, **8**, e83410.
49 R. E. Hershberger, J. Cowan, A. Morales and J. D. Siegfried, *Circ.: Heart Failure*, 2009, **2**, 253–261.
50 C. Ostlund, T. Sullivan, C. L. Stewart and H. J. Worman, *Biochemistry*, 2006, **45**, 1374–1382.
51 J. L. Broers, B. M. Machiels, G. J. van Eys, H. J. Kuijpers, E. M. Manders, R. van Driel and F. C. Ramaekers, *J. Cell Sci.*, 1999, **112**(Pt 20), 3463–3475.
52 T. Shimi, K. Pfleghaar, S. Kojima, C. G. Pack, I. Solovei, A. E. Goldman, S. A. Adam, D. K. Shumaker, M. Kinjo, T. Cremer and R. D. Goldman, *Genes Dev.*, 2008, **22**, 3409–3421.
53 K. C. Toh, N. M. Ramdas and G. V. Shivashankar, *Integr. Biol.*, 2015, **7**, 1309–1317.
54 C. Pack, K. Saito, M. Tamura and M. Kinjo, *Biophys. J.*, 2006, **91**, 3921–3936.
55 N. Naetar, K. Georgiou, C. Knapp, I. Bronshtein, E. Zier, P. Fichtinger, T. Dechat, Y. Garini and R. Foisner, *Elife*, 2021, 10.
56 W. Kabsch and C. Sander, *Biopolymers*, 1983, **22**, 2577–2637.

57 N. Stuurman, S. Heins and U. Aebi, *J. Struct. Biol.*, 1998, **122**, 42–66.
58 C. Aponte-Santamaria, S. Lippok, J. J. Mittag, T. Obser, R. Schneppenheim, C. Baldauf, F. Grater, U. Budde and J. O. Radler, *Biophys. J.*, 2017, **112**, 57–65.
59 M. de Castro Fonseca, J. F. de Oliveira, B. H. S. Araujo, C. Canateli, P. F. V. do Prado, D. P. Amorim Neto, B. P. Bosque, P. V. Rodrigues, J. V. P. de Godoy, K. Tostes, H. V. R. Filho, A. F. Z. Nascimento, A. Saito, C. C. C. Tonoli, F. A. H. Batista, P. S. L. de Oliveira, A. C. Figueira, S. Souza da Costa, A. C. V. Krepischi, C. Rosenberg, H. Westfahl Jr, A. J. R. da Silva and K. G. Franchini, *iScience*, 2021, **24**, 102841.